Rhenium-doped MoS_2 films

Toby Hallam, Scott Monaghan, Farzan Gity, Lida Ansari, Michael Schmidt, Clive Downing, Conor P. Cullen, Valeria Nicolosi, Paul K. Hurley, and Georg S. Duesberg

Citation: Appl. Phys. Lett. **111**, 203101 (2017); doi: 10.1063/1.4995220
View online: https://doi.org/10.1063/1.4995220
View Table of Contents: http://aip.scitation.org/toc/apl/111/20
Published by the American Institute of Physics

Articles you may be interested in

Low sub-threshold swing realization with contacts of graphene/h-BN/MoS_2 heterostructures in MoS_2 transistors
Applied Physics Letters **111**, 193502 (2017); 10.1063/1.4997226

P-type conduction in two-dimensional MoS_2 via oxygen incorporation
Applied Physics Letters **110**, 193103 (2017); 10.1063/1.4983092

A sub-thermionic MoS_2 FET with tunable transport
Applied Physics Letters **111**, 163501 (2017); 10.1063/1.4996953

High performance broadband photodetector based on MoS_2/porous silicon heterojunction
Applied Physics Letters **111**, 191107 (2017); 10.1063/1.5004025

Oxygen-assisted synthesis of hexagonal boron nitride films for graphene transistors
Applied Physics Letters **111**, 203103 (2017); 10.1063/1.5001790

p-type doping of MoS_2 thin films using Nb
Applied Physics Letters **104**, 092104 (2014); 10.1063/1.4867197

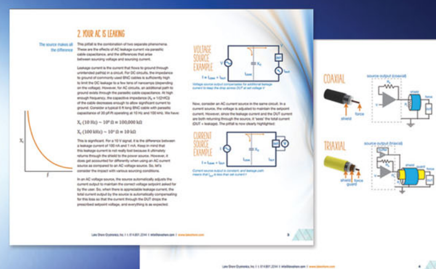

5 Electronic Measurement Pitfalls to Avoid
Get the whitepaper

APPLIED PHYSICS LETTERS 111, 203101 (2017)

Rhenium-doped MoS_2 films

Toby Hallam,[1,2] Scott Monaghan,[3] Farzan Gity,[3] Lida Ansari,[3] Michael Schmidt,[3] Clive Downing,[1] Conor P. Cullen,[1,4] Valeria Nicolosi,[1,4] Paul K. Hurley,[3] and Georg S. Duesberg[1,4,5]
[1]*CRANN/AMBER, Trinity College Dublin, Dublin 2, Ireland*
[2]*School of Physics, Newcastle University, Newcastle-upon-Tyne NE1 7RU, United Kingdom*
[3]*Tyndall National Institute, and the Department of Chemistry, University College Cork, Cork T12R5CP, Ireland*
[4]*School of Chemistry, Trinity College Dublin, Dublin 2, Ireland*
[5]*Universität der Bundeswehr München, 85577 Neubiberg, Germany*

(Received 10 July 2017; accepted 25 October 2017; published online 14 November 2017)

Tailoring the electrical properties of transition metal dichalcogenides by doping is one of the biggest challenges for the application of 2D materials in future electronic devices. Here, we report on a straightforward approach to the n-type doping of molybdenum disulfide (MoS_2) films with rhenium (Re). High-Resolution Scanning Transmission Electron Microscopy and Energy-Dispersive X-ray spectroscopy are used to identify Re in interstitial and lattice sites of the MoS_2 structure. Hall-effect measurements confirm the electron donating influence of Re in MoS_2, while the nominally undoped films exhibit a net *p*-type doping. Density functional theory (DFT) modelling indicates that Re on Mo sites is the origin of the n-type doping, whereas S-vacancies have a p-type nature, providing an explanation for the p-type behaviour of nominally undoped MoS_2 films. *Published by AIP Publishing.* https://doi.org/10.1063/1.4995220

The past few years have witnessed huge advances in the use of transition metal dichalcogenide (TMD) 2D materials in a wide variety of applications such as field-effect transistors (FETs),[1] light harvesting devices,[2] chemical sensors,[3] photocatalysts,[4] and flexible electronics.[5] With the introduction of chemical vapour deposition (CVD) approaches to synthesis, TMD device technology has taken off quickly.[6] For emerging electronic applications, particularly the development of a CMOS analogue, it will be necessary to tune the electronic properties of TMDs through local modulation of the free carrier concentrations, both for the formation of *pn* junctions and minimizing the specific contact resistivity of TMD/metal contacts.

From previous work on TMD materials, physisorption of molecules is known to be a route to controlling the carrier concentration.[7] Physisorption[8] or chemisorption[9] of molecules can lead to a doping effect. However, these treatments are relatively unstable with lifetimes of a few days to a few hours.

The more traditional approach to controlling the carrier concentration is doping through substitution of the transition metal or the chalcogen with appropriate elements.[10] Substitutional doping disturbs the structure of the TMDs through defect formation which could impact transport properties in materials with only a single layer in thickness. However, as the multi-year stability of device electronic properties will be required for practical applications, substitutional doping remains one of the most promising approaches to date.

When looking at appropriate dopants for MoS_2, there are a few candidates. For a complete review, the reader is directed to the recent review by Pham and Yeom.[11] Briefly, Nb is known as a *p*-type dopant theoretically and experimentally.[12–14] However, for *n*-type dopants, the reports are limited.[15] Theoretical work by Dolui *et al.*[12] highlights a number of possible dopants for MoS_2. Re substitution was identified as a good candidate for n-type doping with the lowest activation energy of all of the elements they considered.

There are also experimental reports of Re acting as a dopant in MoS_2: physical vapour transport, based on long growth times (>240 h at 930 °C), has been used to introduce Re to create n-type MoS_2.[16] Electron paramagnetic resonance experiments on natural MoS_2 identified Re behaving as a donor and S vacancies behaving as acceptors.[17] Nb was also introduced into CVD MoS_2 using a metal oxide process[18] and $NbCl_5$, demonstrating modification of the MoS_2 resistivity based on substitution.[19]

These publications demonstrate that Re doping can work in mechanically exfoliated flakes from MoS_2 grown by vapour phase transport or Nb in isolated CVD domains. A natural extension of these works is to explore Re doping in continuous MoS_2 thin films. One simple approach to the formation of TMD materials, in which Re doping has not been explored, is the so-called thermally assisted conversion (TAC) process. Essentially, the process consists in the deposition of a thin layer of a transitional metal which is then exposed to chalcogen vapour. We have reported extensively on this process for the formation of intrinsic TMDs of both metal sulphides[20] and metal selenides.[21] The real advantage of this technique is the opportunity to "scale-up". In this paper, the dimension for samples is at most 1 cm^2. However, both metal film deposition and sulfur vapour annealing are processes that are amenable to application at the wafer scale. By presenting chemical, structural, and electrical characterization of continuous centimetre-scale Re doped MoS_2, we show a feasible route to the fabrication of much larger scale *n*-doped films.

To incorporate rhenium heteroatoms into TAC MoS_2, we follow the work of Laskar *et al.*[13] We confirm the presence of rhenium in both substitutional lattice sites and

interstitial positions using spectroscopy, High Resolution Scanning Transmission Electron Microscopy (HRSTEM), and Energy-Dispersive X-ray spectroscopy (EDX). Both DC and AC magnetic field Hall measurements are used to confirm the electrical activation of rhenium dopants, and density functional theory (DFT) is used to qualitatively explain the complimentary doping behaviour of rhenium and the sulfur-vacancy (S-vacancy).

Figure 1(a) shows a schematic of our process to introduce dopants to MoS_2 where interleaved Mo and Re layers are sulfurized to form a doped film. To create the initial film, we have used alternating sputter deposition of Mo and Re. The Mo:Re films in this paper were created by alternated Mo layers of 12×2 nm thickness and Re layers of 11×0.2 nm thickness such that the total thickness of the film is 26.2 nm of which rhenium takes up 8.4% by volume, and the first and final layers deposited are molybdenum. Substrates were 300 nm SiO_2 on n^{++} Si in all cases except for Hall devices in which we used single crystal Al_2O_3 (00001) to avoid current leakage through the substrate.

In order to promote uniform inter-diffusion of the Mo and Re laminate structure, the films were subject to a 60 min anneal at 900 °C in argon. Re has good solubility in Mo, so it is a reasonable expectation for several nm of diffusion

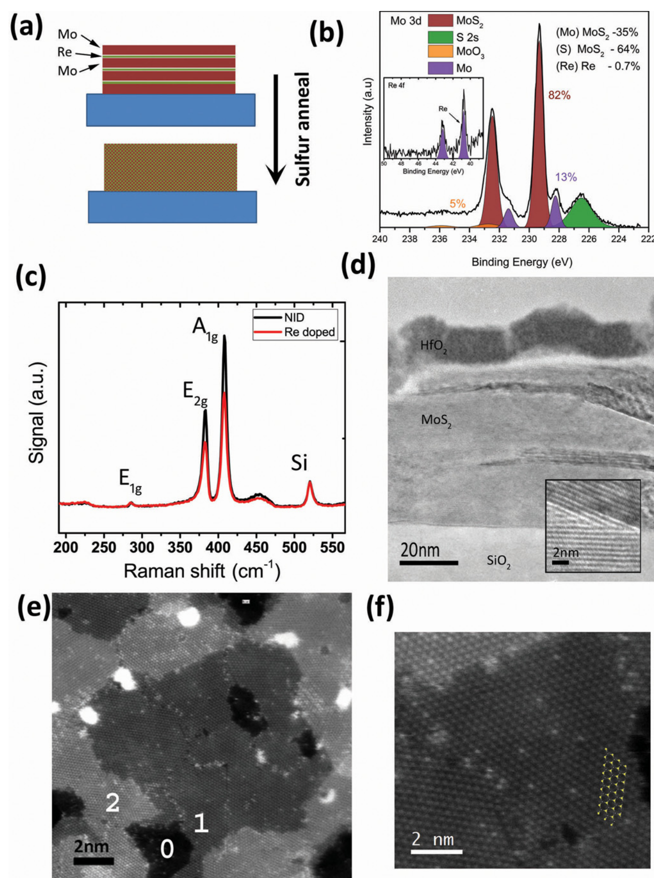

FIG. 1. (a) Schematic showing the initial layered Re:Mo structure diffusing to form a homogeneous film. (b) XPS of the Mo 3d region for the Re-doped MoS_2 film. Inset: Re 4F region. (c) Raman spectra of undoped and doped MoS_2 films. (d) Cross-sectional TEM of the doped MoS_2 film on SiO_2. Inset: Magnified region of the main image. The upper dark layer is the HfO_2 capping layer. (e) HRSTEM of doped MoS_2. Layer numbers identified in white. (f) Close up from (e) where individual Re features can be located in lattice sites as indicated by overlay.

through sputtered thin films.[22] Following the inter-diffusion anneal, the sample is exposed to sulfur vapour as described previously.[20] In this low pressure process (20 mTorr), the metal film is alloyed over the course of 30 min at 900 °C. After the film is removed from the furnace, the total thickness is 55 nm ± 5 nm, indicating a doubling of the initial thickness, which is comparable to our previous results. Thinner MoS_2 films for HRSTEM were created by sputtering thinner initial layers of Re and Mo (0.1 nm Re and 0.7 nm Mo). The film was sulfurized and then transferred to a Transmission Electron Microscopy (TEM) grid using a modified polymer assisted transfer technique.[23]

To investigate the chemistry of the doped samples, we have carried out X-ray photoelectron spectroscopy (XPS) of both the doped and undoped films. Figure 1(b) shows the Mo 3D signals of the doped films. Core-level scans of the Mo 3d, S 2p, and Re 4f regions were taken to analyse the amount, and chemical configuration, of different components. The analysis of the Mo 3d core level reveals three distinct components, with large amounts of MoS_2, alongside much smaller quantities of elemental Mo and MoO_3. The S 2p core-level analysis confirmed the correct stoichiometry for MoS_2, indicating complete conversion. The Re 4f core-level region confirmed the presence of elemental Re in the sample. XPS indicates that these Re atoms are not bound to any particular atom and exist in their elemental form. A concentration of ~1 Re atom per 100 Mo atoms is calculated by comparison of the relative area, and sensitivity, of the relevant core levels. This value is lower than expected, considering that approximately 8 vol. % of the original metal content was Re. One possible explanation is that XPS is a highly surface sensitive spectroscopic technique, and a signal is only obtained from the top 2–10 nm of the film. If the Re concentration exhibits a spatial variation due to incomplete mixing of Mo and Re during annealing, this could lead to a low concentration at the surface, especially as Mo is the final layer deposited in the Mo:Re laminate structure prior to the sulfur exposure process. Furthermore, the low signal level for Re in this sample gives an estimated error of 1%–2%. Regardless of the concentration, Re is positively identified in the sample.

Raman spectroscopy was also used to examine doped and undoped films. Figure 1(c) shows overlaid spectra from both samples. While the spectrum does show the bulk Raman signature of MoS_2 (E1g, E2g, and A1g),[24] it does not show those of ReS_2 at 163 cm^{-1} (E2g) and 213 cm^{-1} (A1g-like).[25] Hence, there is no strong phase segregation of the MoS_2 and ReS_2 systems. We assume that this probe is a measure of a significant portion of the composite systems as the penetration depth at 532 nm incident wavelength is expected to be 20–30 nm,[26] compared to the total film thickness of 55 nm.

While the XPS and Raman probes give us aggregate information about the chemical composition of the films, they do not illuminate the material morphology. We conducted HRTEM of cross sections and HRSTEM measurements of specially created few layer films to provide complimentary information about the nature of the Re dopants in MoS_2 films. Figure 1(d) shows a cross-sectional TEM image and indicates a mostly uniform 2D layered film of approximately 55 nm thickness. This particular Re doped MoS_2 film had a capping

layer of HfO_2 deposited on the surface by electron beam evaporation. One can see the overall aligned basal planes of MoS_2 parallel to the substrate. It is also apparent that the film is composed of adjoining grains. The grains show a similar lattice spacing of 6.3 Å, indicating that they are grains of the same material oriented at different angles around the main orientation perpendicular to the growth direction. Pristine MoS_2 has a lattice spacing of 6.15 Å, indicating that the Re dopant could cause it to increase to 6.3 Å in the observed material. An AFM surface image of an identically prepared Re doped MoS_2 sample (without a HfO_2 capping layer) can be seen in Fig. S1 (supplementary material).

The image in Fig. 1(e) shows a plan view HRSTEM image of the thin Re-doped MoS_2 film (∼1.5 nm) transferred onto a TEM grid. The sample consists of an almost continuous film of highly crystalline MoS_2. Different regions have different layer numbers (representative regions have been identified as 0, 1, and 2 corresponding to layer numbers). From the Moiré patters in the multi-layer regions, we can see that there is no overall preferred stacking as is expected from the TAC growth approach. Furthermore, large bright white circular features are visible. These can be identified by atomic scale EDX as rhenium and rhenium oxides.

Looking more closely at the lattice, it can be seen that in addition to the MoS_2 atoms, there are numerous small bright spots. These bright features are observed in two locations: In a high concentration at the grain boundaries and a lower concentration in lattice sites. We propose that these are Re atoms due to an expected Z-contrast with Mo, but we have used EDX to confirm the assertion. EDX identification tags are overlaid onto an HRSTEM image in Fig. S2 (supplementary material). While the statistics are somewhat limited, EDX confirms that the Re signal is localized only in the regions with the bright contrasting feature observed in HRSTEM.

Using the atomically resolved capability of our aberration corrected STEM, we are able to zoom in on the bright Re features in Fig. 1(f) to determine if they sit in lattice sites or interstitially. A ball and stick overlay shows that the Re atoms within grains sit at Mo lattice sites, whereas those found at grain boundaries are interstitial and often streaky. The streaky features are due to mobile atoms that are not bound to the lattice, confirming their interstitial nature.

To compliment chemical and morphological investigations, we also carried out Hall-effect measurements. Samples for Hall analysis were made from films fabricated identically to those described above with the addition of Ti/Au contacts in a van der Pauw configuration. The inset in Fig. S3 (supplementary material) shows a photograph of such a device. The TMD material (dark region in the centre) has a square area of 0.25 cm^2. A typical 2-point I–V measurement is shown in Fig. S3 (supplementary material). The general linear behaviour was found in all samples, indicating good Ohmic contacts. All devices exhibited resistivity within the range of ∼5–50 Ω.cm as shown in Table I.

From four point current-voltage measurements and Hall measurements, we determine the resistivity, the majority carrier type, the carrier density, and the Hall mobility of the TMD material. These films were grown on single crystal Al_2O_3 (0001). To ensure reproducibility, we created 3 Hall devices with no intentional doping (termed NID#1–3). In these devices, only molybdenum was deposited (initial thickness, 26 nm) and then alloyed with sulfur. In addition and again to ensure reproducibility, 3 Re:Mo Hall devices were deposited and sulfurised as described previously (termed Re#1–3). In all other respects, the devices, contacting the method and substrate, were identical. Devices were made on different occasions over the course of 3 months.

TABLE I. Hall effect data for non-intentionally doped (NID) and rhenium doped (Re) samples.

Sample name	Carrier type	Resistivity (Ω cm)	Hall Coefficient (cm^3/C)	Hall Mobility (cm^2/V s)	Carrier Conc. (cm^{-3})
NID#1	P	3.96	41.83	0.11	1.5×10^{19}
NID#2	P	15.57	2.45	0.16	2.6×10^{18}
NID#3	P	30.11	18.61	0.62	3.4×10^{17}
Re#1	N	27	11.04	0.41	5.7×10^{17}
Re#2	N	9.73	6.83	0.7	9.1×10^{17}
Re#3	N	52.98	7.2	0.14	8.7×10^{17}

Both DC and AC magnetic field (B) Hall-effect measurements of non-intentionally doped films indicate a *p*-type semiconductor, where the *p*-type doping concentrations vary between $\sim 3 \times 10^{17}$ cm^{-3} and 1×10^{19} cm^{-3}. The hole mobility values are in the range of 0.1 to 0.6 cm^2/V s (see Table I). The net *p*-type doping was observed for all non-intentionally doped MoS_2 films. One possible source of this net *p*-type behaviour is the presence of S-vacancies which are known to be present in MoS_2 films and exfoliated flakes.[27] This is examined later in this paper using density functional theory calculations.

The Re-doping of the MoS_2 samples is observed to consistently lead to a net *n*-type doping. The free carrier concentration in the Re-doped MoS_2 is in the mid to high 10^{17} cm^{-3} range for all Re-doped MoS_2 samples, compared to the high variability of the hole concentration recorded on the undoped MoS_2 sample. The electron mobility values are in the range of 0.1 to 0.7 cm^2/V s. The percentage activation of Re is very low (around 0.001%), and it can be reasonably assumed that the low activation is related to the low volume density of Re atoms which sit on substitutional Mo sites (as observed in the high resolution EDX in Fig. S2 in the supplementary material).

Re as a dopant in MoS_2 is also investigated through atomic scale simulations by substitutionally replacing a Mo atom in pristine MoS_2 by a Re atom. It is noted that the aim of the atomic scale simulations was to explore if the inclusion of Re on the Mo lattice site results in a movement of the Fermi level (E_F) towards the MoS_2 conduction band, as opposed to an attempt to simulate the active electron concentrations observed experimentally, which are in the mid to high 10^{17} cm^{-3} range. The supercell size required to simulate Re concentrations in the 10^{17} cm^{-3} range is prohibited by computation time.

The simulated structure consists of a single Re impurity in a supercell with 192 atoms which creates a relatively high doping concentration of $\sim 3.1 \times 10^{20}$ cm^{-3}. The band structure of the pristine and Re-doped MoS_2 for the aforementioned concentration is shown in Figs. 2(a) and 2(b), respectively. As can be seen, the Fermi level (E_F) of the Re-doped MoS_2 is

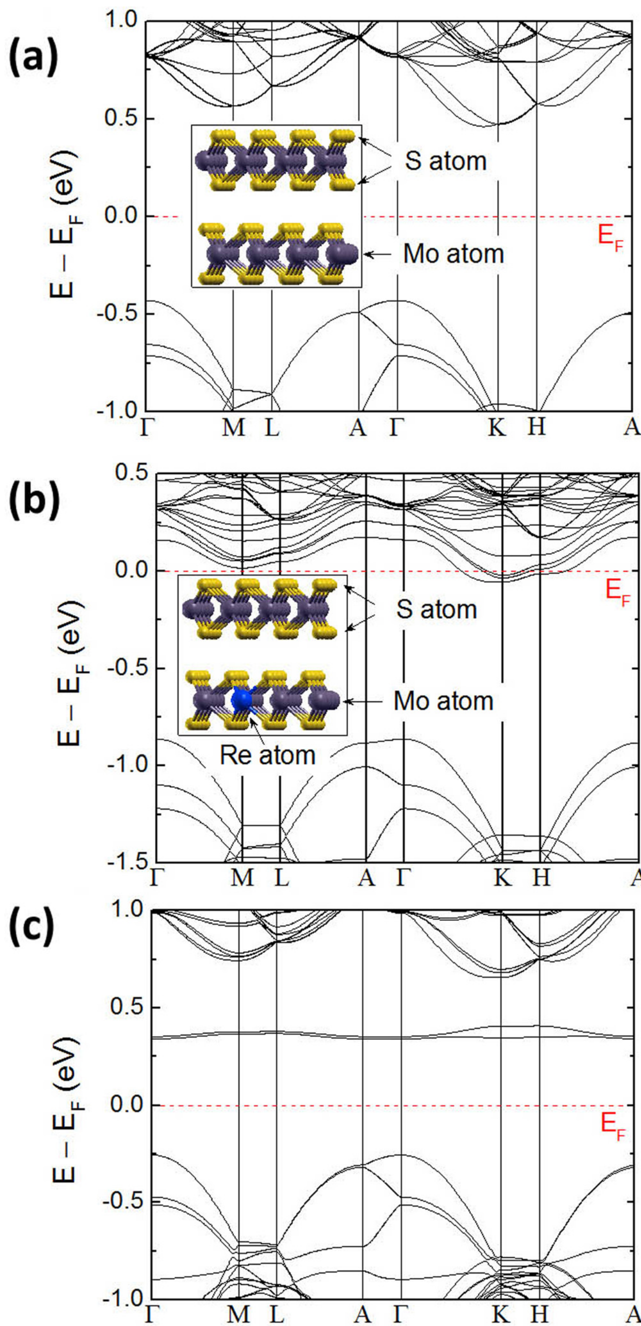

FIG. 2. Band structures calculated from first-principles density functional theory (DFT) for (a) pristine, (b) Re-doped MoS_2 with the doping concentration of $\sim 3.1 \times 10^{20}\,cm^{-3}$, and (c) MoS_2 structure with a S-vacancy showing defect-induced double electronic states in the bandgap. The insets in (a) and (b) show the atomic illustration of the structures. The red dashed lines are the Fermi energy (E_F) level. Energies are referenced to the Fermi level.

heavily shifted from its original position for the pristine MoS_2, i.e., mid-gap, towards the conduction band. Due to the high concentration of Re, its energy level is within the conduction band (degenerate condition). This shift in E_F confirms the *n*-type behaviour of the Re-doped MoS_2 films presented in Table I. The simulated concentration of Re was very large ($10^{20}\,cm^{-3}$) compared to that measured in our doped samples (10^{17} to $10^{18}\,cm^{-3}$) due to computational limitations. However, the E_f shift is consistent with electron donation, supporting our assertion that we have substitutional Re atoms that are n-doping the material.

In order to understand the origin of the observed *p*-type behaviour of the NID MoS_2 films (see Table I), we have performed DFT calculations considering a single S-vacancy where the point defects are more than 13 Å apart. The band structure of MoS_2 with an S-vacancy in the 192 atom supercell at room temperature is shown in Fig. 2(c), indicating that the Fermi level is closer to the valence band edge corresponding to the acceptor-type dopant nature of the NID MoS_2 films. There is a double defect-induced electronic mid-gap state due to this S-vacancy (see Fig. S4 in the supplementary material for the projected density of states—PDoS), comparing the density of states adjacent to and away from the S-vacancy. In a recent study, it has been shown that single sulfur atom vacancies are the dominant defects in the exfoliated single layer of MoS_2, generating similar states in the bandgap.[28] At low temperatures where the Fermi distribution is close to the step-like function, less charges will be captured by the S-vacancy-induced energy state due to losing thermal energy, causing E_F to move towards the mid-gap level (the band structure at 10 K is shown in Fig. S5 in the supplementary material).

We used TAC to create electrically viable MoS_2 films on a large scale. The formation of MoS_2 with TAC leads to films with a small domain size in the range of 50–100 nm (Ref. 21) where a large amount of the material is involved in grain boundaries. In these regions, an abundance of sulfur vacancies is expected. This is confirmed by the observation of several distinct domains in cross-sectional TEM. Our DFT modelling and that of others[29] have indicated that S-vacancy in MoS_2 behaves as a *p*-type dopant. In addition, XPS shows that the chemical composition notably includes molybdenum-oxygen structures. This can be expected from previous results and atmospheric exposure of the material. Oxygen is also known to shift the behaviour of MoS_2 to the *p*-type.[30] So, it is well expected that the overall behaviour of large scale NID MoS_2 films is of *p*-type. This unintentional doping further shows a large variation in the Hall coefficient and resulting doping levels in the materials which vary by several orders of magnitude across several devices. We believe that variations in the furnace such as S partial pressure lead to this variation. Other reports with a very high S partial pressure have shown more consistent doping levels in pristine MoS_2.[13]

On the other hand, the intentional introduction of Re as a dopant to our MoS_2 creates consistent *n* type carrier concentrations in our Hall measurements. We intentionally introduced a very large amount of Re into MoS_2. The result of this over-dosing was that while some Re was incorporated in lattice sites, the majority sat interstitially at grain boundaries and some segregated into regions of elemental Re. We were able to not only observe this behaviour specifically in HRSTEM but also confirm it within the XPS accuracy ($\sim$0.5%) where we would only expect the elemental rhenium to be observed.

Electrical Hall measurements showed that for Re-doped MoS_2, the doping level was consistent and of *n*-type. This is supported by DFT modelling that shows that Re acts as an *n*-type dopant. This is also in line with other experimental observations of Re substituted MoS_2.[17] However, this does not address the balanced counter-doping of the S-vacancy and oxygen defects. It is possible that the high proportion of

interstitial or poorly coordinated Re atoms, predominantly at the grain boundaries, are responsible for neutralizing the high density of S-vacancy acceptors.

In conclusion, we have demonstrated the scalable synthesis of *n*-doped MoS_2 films with Re. During the TAC process of the Mo-Re alloy, no phase segregation was observed. Some of the Re atoms are incorporated into the MoS_2 lattice. Using XPS and HRSTEM, we were able to identify the included Re atoms in elemental or interstitial configurations. As a result, we were able to reproducibly synthesise *n*-doped MoS_2 films with carrier concentrations in the range of 5×10^{17} cm^{-3} to 9×10^{17} cm^{-3} from Hall measurements and supported by DFT studies. The carrier mobility values of the films are in the range of 0.1 to 0.7 cm^2/V s. The TAC of alloys is a universal avenue for further research into doped TMD materials, which are considered for the future of 2D electronics.

See supplementary material for additional details concerning experimental methods (synthesis, XPS, Raman, TEM, Hall, and DFT). Also included is additional experimental data (AFM and TEM) and DFT modelling (PDoS and band structure).

The authors acknowledge SFI Grant Nos. 12/RC/2278, PI_15/IA/3131, European Commission grant 696656 (Graphene Flagship) and support of the Intel Corporation.

[1]Y. Yoon, K. Ganapathi, and S. Salahuddin, Nano Lett. **11**(9), 3768 (2011).
[2]M. S. Choi, D. Qu, D. Lee, X. Liu, K. Watanabe, T. Taniguchi, and W. J. Yoo, ACS Nano **8**(9), 9332 (2014).
[3]S. Varghese, S. Varghese, S. Swaminathan, K. Singh, and V. Mittal, Electronics **4**(3), 651 (2015).
[4]M. Q. Wen, T. Xiong, Z. G. Zang, W. Wei, X. S. Tang, and F. Dong, Opt. Express **24**(10), 10205 (2016).
[5]J. Pu, L.-J. Li, and T. Takenobu, Phys. Chem. Chem. Phys. **16**(29), 14996 (2014).
[6]H. Schmidt, F. Giustiniano, and G. Eda, Chem. Soc. Rev. **44**(21), 7715 (2015).
[7]D. Kiriya, M. Tosun, P. Zhao, J. S. Kang, and A. Javey, J. Am. Chem. Soc. **136**(22), 7853 (2014).
[8]H. Fang, S. Chuang, T. C. Chang, K. Takei, T. Takahashi, and A. Javey, Nano Lett. **12**(7), 3788 (2012).
[9]L. Yang, K. Majumdar, H. Liu, Y. Du, H. Wu, M. Hatzistergos, P. Y. Hung, R. Tieckelmann, W. Tsai, C. Hobbs, and P. D. Ye, Nano Lett. **14**(11), 6275 (2014); P. Zhao, D. Kiriya, A. Azcatl, C. Zhang, M. Tosun, Y.-S. Liu, M. Hettick, J. S. Kang, S. McDonnell, S. Kc, J. Guo, K. Cho, R. M. Wallace, and A. Javey, ACS Nano **8**(10), 10808 (2014).
[10]J. Suh, T.-E. Park, D.-Y. Lin, D. Fu, J. Park, H. J. Jung, Y. Chen, C. Ko, C. Jang, Y. Sun, R. Sinclair, J. Chang, S. Tongay, and J. Wu, Nano Lett. **14**(12), 6976 (2014); A. A. Tedstone, D. J. Lewis, and P. O'Brien, Chem. Mater. **28**(7), 1965 (2016).
[11]V. P. Pham and G. Y. Yeom, Adv. Mater. **28**(41), 9024 (2016).
[12]K. Dolui, I. Rungger, C. Das Pemmaraju, and S. Sanvito, Phys. Rev. B **88**(7), 075420 (2013).
[13]R. Laskar Masihhur, N. Nath Digbijoy, M. Lu, W. Lee Edwin II, L. C. Hee, K. Thomas, Y. Zihao, M. Rohan, A. Roldan Manuel, I. Juan-Carlos, T. Pantelides Sokrates, J. Pennycook Stephen, C. Myers Roberto, W. Yiying, and R. Siddharth, Appl. Phys. Lett. **104**(9), 092104 (2014).
[14]M. Gioele, S. Michael, S. Brendan, C. Karim, M. Scott, P. Ian, M. L. MCarthy, P. Bell Alan, N. Roger, C. Felice, K. Hurley Paul, and D. Ray, AIP Adv. **6**(2), 025323 (2016).
[15]H.-Y. Park, M.-H. Lim, J. Jeon, G. Yoo, D.-H. Kang, S. K. Jang, M. H. Jeon, Y. Lee, J. H. Cho, G. Y. Yeom, W.-S. Jung, J. Lee, S. Park, S. Lee, and J.-H. Park, ACS Nano **9**(3), 2368 (2015); D.-H. Kang, S.-T. Hong, A. Oh, S.-H. Kim, H.-Y. Yu, and J.-H. Park, Mater. Res. Bull. **82**, 26 (2016).
[16]K. K. Tiong, P. C. Liao, C. H. Ho, and Y. S. Huang, J. Cryst. Growth **205**(4), 543 (1999).
[17]F. D. Brandão, G. M. Ribeiro, P. H. Vaz, J. C. González, and K. Krambrock, J. Appl. Phys. **119**(23), 235701 (2016).
[18]Y.-C. Lin, W. Zhang, J.-K. Huang, K.-K. Liu, Y.-H. Lee, C.-T. Liang, C.-W. Chu, and L.-J. Li, Nanoscale **4**(20), 6637 (2012).
[19]N. Al-Dulaimi, D. J. Lewis, X. L. Zhong, M. Azad Malik, and P. O'Brien, J. Mater. Chem. C **4**(12), 2312 (2016); J. Gao, Y. D. Kim, L. Liang, J. C. Idrobo, P. Chow, J. Tan, B. Li, L. Li, B. G. Sumpter, T.-M. Lu, V. Meunier, J. Hone, and N. Koratkar, Adv. Mater. **28**(44), 9735 (2016).
[20]R. Gatensby, N. McEvoy, K. Lee, T. Hallam, N. C. Berner, E. Rezvani, S. Winters, M. O'Brien, and G. S. Duesberg, Appl. Surf. Sci. **297**, 139 (2014).
[21]R. Gatensby, T. Hallam, K. Lee, N. McEvoy, and G. S. Duesberg, Solid-State Electron. **125**, 39 (2016).
[22]R. Mathieu, N. Dupin, J. C. Crivello, K. Yaqoob, A. Breidi, J. M. Fiorani, N. David, and J. M. Joubert, Calphad **43**, 18 (2013).
[23]C. Yim, M. O'Brien, N. McEvoy, S. Riazimehr, H. Schäfer-Eberwein, A. Bablich, R. Pawar, G. Iannaccone, C. Downing, G. Fiori, M. C. Lemme, and G. S. Duesberg, Sci. Rep. **4**, 5458 (2014).
[24]C. Lee, H. Yan, L. E. Brus, T. F. Heinz, J. Hone, and S. Ryu, ACS Nano **4**(5), 2695 (2010).
[25]S. Tongay, H. Sahin, C. Ko, A. Luce, W. Fan, K. Liu, J. Zhou, Y.-S. Huang, C.-H. Ho, J. Yan, D. F. Ogletree, S. Aloni, J. Ji, S. Li, J. Li, F. M. Peeters, and J. Wu, Nat. Commun. **5**, 3252 (2014).
[26]D. V. Voronine, G. Lu, D. Zhu, and A. Krayev, IEEE J. Sel. Top. Quantum Electron. **23**(1), 4600506 (2017).
[27]W. Zhou, X. Zou, S. Najmaei, Z. Liu, Y. Shi, J. Kong, J. Lou, P. M. Ajayan, B. I. Yakobson, and J.-C. Idrobo, Nano Lett. **13**(6), 2615 (2013).
[28]P. Vancsó, G. Z. Magda, J. Pető, J.-Y. Noh, Y.-S. Kim, C. Hwang, L. P. Biró, and L. Tapasztó, Sci. Rep. **6**, 29726 (2016).
[29]D. Liu, Y. Guo, L. Fang, and J. Robertson, Appl. Phys. Lett. **103**(18), 183113 (2013); M. Houssa, K. Iordanidou, G. Pourtois, V. V. Afanas'ev, and A. Stesmans, Appl. Surf. Sci. **416**, 853 (2017).
[30]C. Mikai, N. Hongsuk, W. Sungjin, J. Lian, R. Xin, B. Lifeng, L. Shulong, and L. Xiaogan, Appl. Phys. Lett. **103**(14), 142110 (2013).